The 2009 IEEE/RSJ International Conference on
Intelligent Robots and Systems
October 11-15, 2009 St. Louis, USA

Penetration Force Measurement and Control in Robotic Cell Microinjection

Yu Xie, Dong Sun, *Senior Member, IEEE*, and Chong Liu

***Abstract*—In a robotic cell injection system, the penetration force applied on the cell reflects the changes of the physical behavior of the cell. The force, if not controlled properly, may damage to the cells or even lead to death of the cells. The current cellular force measurement is limited by the inherent cantilever structure of the sensor, which may not be applicable to a practical cell injection system. In this paper, a simply supported beam structure based PVDF force sensor is first presented. The proportion relation is established between the penetration force and the sensor output after compensation. Using the designed force sensor, the force applied on the cell can be measured, and a force control based cell injection system is constructed. The experimental results performed on zebrafish embryos demonstrate the effectiveness of the micro force sensor and the force based control framework.**

I. Introduction

With the advent of systems biology, the need for testing genetic materials far exceeds the biological community's current capability. One of the obstacles is the current lack of high through-put technology platform to introduce genetic materials into whole organisms. The advent of automatic injection system will greatly add to the scoped of possible microinjection experiments [1].

Microinjection of microliters of genetic materials into fish embryo is a standard procedure used to test the functions of the introduced genetic materials on the survival and development of embryos [2] [3]. In a robotic injection system, the microinjector is driven toward the cell with high accuracy and repeatability a certain time. Among the existing automatic injection systems reported in the literature, injection methods can be divided into visual position feedback [4]-[6] and force feedback [7]-[9]. Force feedback is usually more effective than the visual position feedback, because direct force information reflects the changes of the physical behavior of the cell (i.e. deformation or extent of penetration) more quickly and accurately [7]. On the other hand, it is known that a successful cell injection task is related not only to the successful injection itself but also to whether the living cell can survive after injection. During the penetration procedure, if the applied force exceeds a certain threshold, mechanical injury results. The penetration force measurement and control, therefore, play important roles in a robotic cell injection system, indicating increasing importance of interaction control in cell manipulation [10].

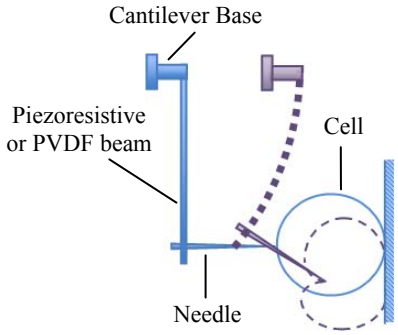

Fig. 1. A typical cantilever structure based PVDF force sensor.

Using a piezoelectric or piezoresistive material as a sensing element of a force sensor has been reported in many applications. An atomic force microscope (AFM) is a typical application with a piezoelectric or piezoresistive cantilever structure to sense the nano-newton forces [11] [12]. The force required to penetrate a fish embryo has been found in the range of micro Newton [7] [8] [13]-[17]. Preliminary works have been carried out to prove the feasibility of using a piezoelectric or piezoresistive force sensor in a micro newton range. In application of biological cell manipulation, for instance, Lu et al. used a piezoresistive force sensor to monitor the zebra fish embryo injection process, where the real time force signal was used to determine the stop moment since the force exhibits an obvious decline when a cell was penetrated [7]. To study the mechanical property of a fruit fly embryo, Wejinya et al. used a piezoelectric PVDF (Polyvinylidene Fluoride) film to fabricate a 2-D micro force sensor [13]. Pillarisetti et al. used a PVDF force sensor to evaluating the effect of the force (haptic) feedback in cell injection [14].

Similar to an AFM, the force sensing structures of these works are based on cantilever beam structure, as shown in Fig. 1. A needle is bonded to the free end of cantilever, while the cantilever base is mounted on the manipulator. For cell microinjection, however, such a structure exhibits two obvious disadvantages. The first is that the injected sample is hard to be transferred from the pressure tube to the needle. If the needle is connected to the pressure tube, the gravity of the pressure tube is dominant and far bigger than micro-newton level penetration force. Another disadvantage is that the bending of the cantilever produces bigger puncture wound to the cell than that by a conventional injection process without

This work was supported by a grant from Research Grants Council of the Hong Kong Special Administrative Region, China [Reference No. CityU 120709], UGC Special Equipment Grant [SEG_CityU 01], and a grant from City University of Hong Kong [Reference No. 9360131].

Y. Xie, D. Sun and C. Liu are with the Department of Manufacturing Engineering and Engineering Management, the City University of Hong Kong, Hong Kong (Phone: 852-2194-2927; Fax: 852-2788-8423; e-mail: yuxie2@student.cityu.edu.hk { medsun, chongliu}@cityu.edu.hk).

force measurement.

To overcome these limitations, in this paper we fabricate a new PVDF force sensor for a force feedback cell injection system. Instead of a cantilever beam structure used in most of existing micro force sensors, a simply supported beam is adopted to realize the sample injection. The quantitative relationship between the injection force and the sensor output is derived theoretically. Using the designed force sensor to measure the force applied on the cell, a force control based cell injection system is constructed. Experiments performed on zebrafish embryos demonstrate the effectiveness of the micro force sensor and the force based control framework.

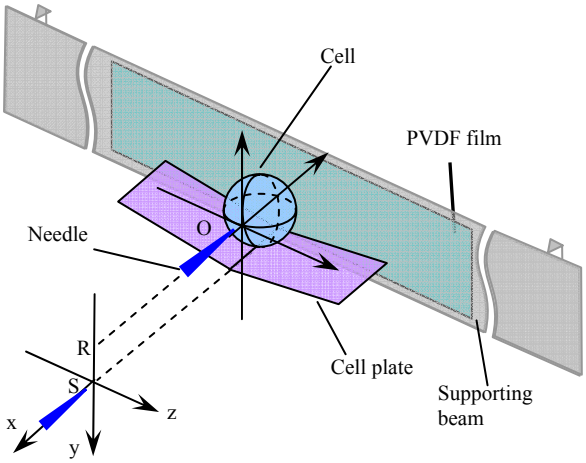

Fig. 2. The beam structure of the PVDF force sensor (O-contact position).

II. Design and Modeling

A. Sensor Description

The PVDF force sensor adopts a simply supported beam structure, as shown in Fig. 2. A PVDF force film (MSI Co. Ltd., model LDT2-28K) is adhesively bonded to the back of the supporting beam. The cell plate is well placed on the beam, so that the center points of the beam, the PVDF film and the cell coincide with each other. When the needle penetrates into the cell along the extension line of RO (see Fig. 2), the process can be considered as a quasi static process. According to Newton's law, the cell penetration force equals the force applied on the PVDF film.

The simplified diagram of the penetration force sensing mechanism is illustrated in Fig. 3. A PVDF film has high DC output impedance and appears as a charge source. Thus, a charge amplifier is needed to convert the charge output from the PVDF film into a voltage signal. Following the charge amplifier, low-pass amplifiers are added to remove the noise in the circuit and amplify the weak voltage signal. A 12-bit analog-digital converter (ADC) then feeds the force signal to the control system. In addition to the low pass filters, shielding techniques are considered to prevent the EMI (electromagnetic interference) noise.

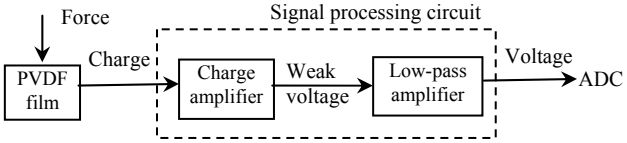

Fig. 3. Sensing mechanism of the PVDF force sensor.

B. Sensor Modeling

PVDF force sensors are active transducers, directly converting applied mechanical energy into electrical energy. In this section, the mathematical model is first derived by defining the deformation of the supporting beam under the applied force F. Then, an electrical transfer function is developed by modeling the signal processing circuit.

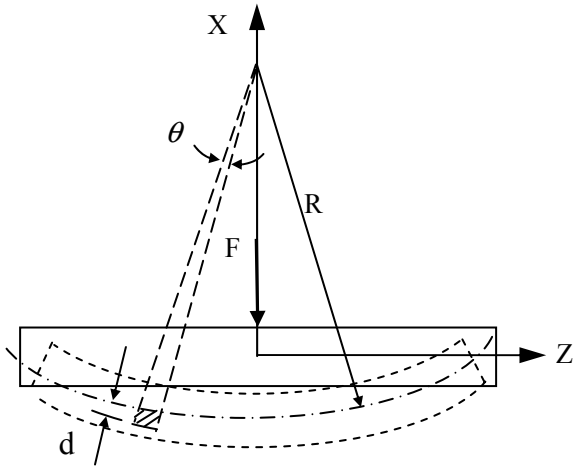

Fig. 4. Deflection of a simply supported beam with a concentrated load.

1) Modeling of the sensing tool

In order to obtain the transfer function between the cell force F and the deformation of the supporting beam, it is important to know where the applied force is acting on the beam. For clear illustration, Fig. 2 is redrawn in Fig. 4 by rotating the beam. A simply supported beam with length $2L$, thickness $2h$, and width $2W$ is considered. Since the force F acts in the center of the beam, the bending moment in the y direction is given by

$$M_y(z) = \frac{F}{2}(L - z) \tag{1}$$

Define that R is the radius of the curvature of the neutral axis, the strain in a small element at a distance d from the neutral axis of the bent beam is derived as

$$e_z = \frac{(R+d)\theta - R\theta}{R\theta} = \frac{d}{R} = -\frac{x}{R} \tag{2}$$

Regarding deformations in the $x-$ and $y-$directions of the beam, it is apparent that changes in the length will result in changes in the transverse directions [18]. The strains will be

$$e_x = e_y = \frac{\mu x}{R} \tag{3}$$

where μ is Poinson's ratio of the beam.

According to Hook's law and (2), the stress in the z direction is

$$\delta_z = -\frac{Ex}{R} \tag{4}$$

where E is the Young's modulus of the beam.
Thus the bending moment in the y direction is expressed as

$$M_y = -\int_s x\delta_z d_x d_y = \frac{E}{R}\int_s x^2 dxdy = \frac{EI}{R} \tag{5}$$

where I is the inertial moment of cross-sectional area.
Using (1) and (5), we have

$$R = -\frac{EI}{M_y} = \frac{2EI}{F(L-z)} \tag{6}$$

Substitute (6) into (2) and (3), the strain of the simply supported beam is thereby obtained

$$\begin{cases} e_x = e_y = \dfrac{\mu F(L-z)x}{2EI} \\ e_z = \dfrac{F(z-L)x}{2EI} \end{cases} \tag{7}$$

Noting that the PVDF film is stuck at the bottom of beam, hence for the PVDF film, we have

$$e_x\big|_{x=-h} = \frac{-\mu F(L-z)h}{2EI} \tag{8}$$

Eq. (8) implies that the applied force F is strictly linear to the strain in the x direction. On the other hand, refer to [19] the charge produced by PVDF film is proportional to strain and increases linearly with the sensor surface. Therefore, the proportional relation between the force F and charge Q is obtained.

2) Modeling of the signal processing circuit

The home-made signal processing circuit composes of a charge amplifier and a low-pass amplifier. The electronic circuit of the charge amplifier is presented in Fig. 5. The parallel RC in the feedback loop has impedance

$$Z = \frac{R_f}{1 + j\omega R_f C_f} \tag{9}$$

where ω is the frequency of the input signal.
Then the output voltage V_C subjected to the input current dQ/dt is obtained

$$V_C = \frac{R_f}{1 + j\omega R_f C_f}\frac{dQ}{dt} \tag{10}$$

By Laplace transformation, the electrical transfer function for charge amplifier is

$$V_C = \frac{R_f s}{1 + R_f C_f s} Q \tag{11}$$

The time constant $\tau = R_f C_f = 1\text{sec}$ with a selection of $R_f = 100M\Omega$ and $C_f = 10nF$. Combining to the low pass amplifier, the transfer function of the complete signal processing circuit is give as

$$V = kV_C \tag{12}$$

where k is the gain of the low pass amplifier.

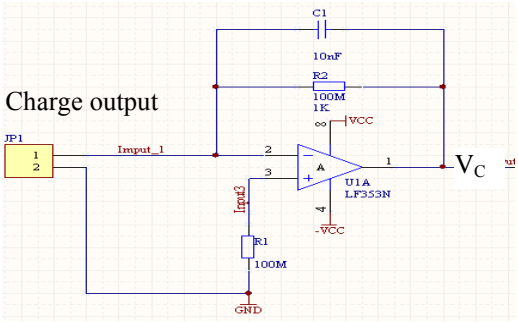

Fig. 5. Electrical circuit of the charge amplifier.

It is worth to note that the force signal used in cell injection is in the low frequency, such as ramp signal. So we cannot simply suppose the output voltage V_C is linear to the charge Q by ignoring the $R_f C_f s$ item as other works, e.g. [14] [15]. To let the sensor output proportional to the force input, a compensator $\frac{1+s}{s}$ is thereby added.

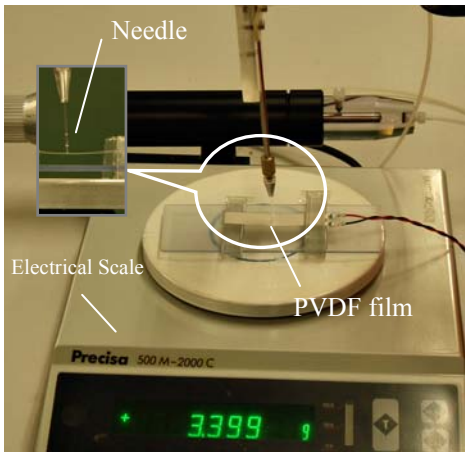

Fig. 6. Calibration setup for the force sensor.

C. *Sensing Performance*

To validate the effectiveness of the integrated force sensor and the previous consideration, a simple experimental setup is built, as shown in Fig. 6. It can be seen that the needle is vertically aligned on the PVDF beam. The PVDF force sensor is placed on a precision electrical scale (Precisa Gravimetrics AG, Model: 500M-2000C) with a measurement range of 500g and a resolution of 0.001g.

When a manipulator moves toward the PVDF beam, the force exerted to the film equals the one to the electrical scale. Five different displacements are executed, while each displacement has three or four trials. The results demonstrate good linearity between the sensor deflection and force input, as shown in Fig. 7.

Fig. 8 presents the ADC output of the sensor under a constant force 1220 μN. It can be observed that if the electrical transfer function is not compensated, the force signal will change as the time elapse. By comparison, we can

see that red dash line maintain a good steady property value with compensation.

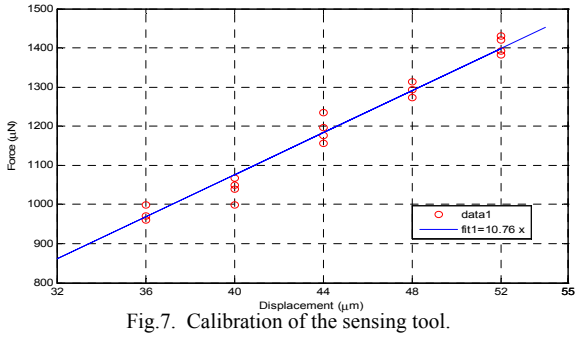

Fig.7. Calibration of the sensing tool.

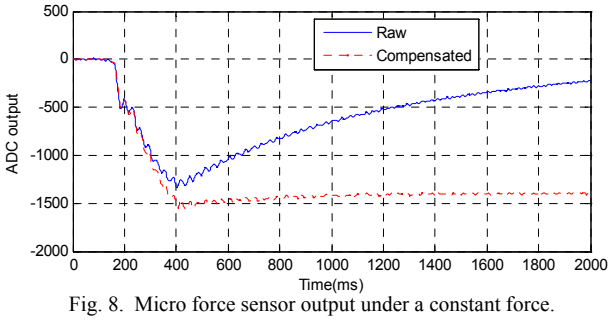

Fig. 8. Micro force sensor output under a constant force.

III. FORCE FEEDBACK CONTROL SYSTEM

A. System Architecture

The designed automated cell injection system consists of four parts: controller, force sensor, vision unit, and injection unit, as depicted in Fig. 9. The vision unit includes an optical microscope, lighting system, CCD camera, PCI image capture and processing card. The micro force sensor is used to measure the penetration force applied on the cell. The injection unit includes a XYZ positioning table and a microinjector installed on it. The controller includes position and force controls. The position control is used to drive the needle to approach the cell from the start position. When the needle contacts the cell, the control scheme is switched to a force control mode such that the needle penetrates the cell by following the reference force trajectory. Fig. 10 illustrates the integrated cell injection system.

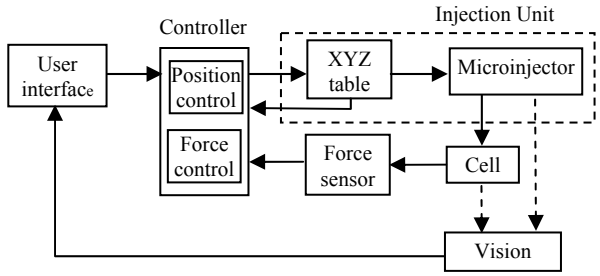

Fig. 9. Schematic of the cell injection system.

B. Force Feedback Control Scheme

Cell injection involves the interaction between the needle and the deformable biological cell. Interaction control strategies can be grouped in two categories: indirect force control and direct force control [20]. The main difference between the two categories is that the indirect force control achieves a force control via a motion control, which is typically available in a robot manipulator; while with the direct force controlled, the force is controlled directly by commanding the joint torques of the robot based on the sensed force error. In the case of biological cell injection, an indirect force control (i.e. impedance control approach [21] [22]) can maintain a desired dynamic relationship between the position of the needle and the external force exerted by the needle on the cell. The advantage of the impedance control is that the transient response of the needle towards the cell can be prescribed by specifying the impedance parameters. To minimize the damage to the cell, the oscillation and overshoot in the transient response should be avoided designing the impedance parameters.

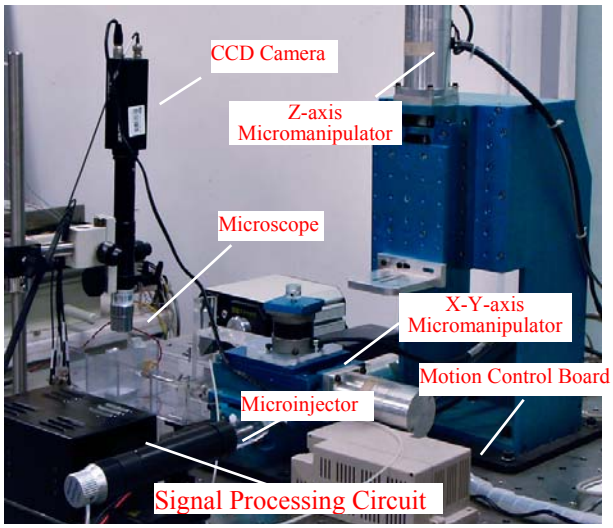

Fig. 10. The integrated cell injection system.

In order to regulate the needle to track a reference force f_r in addition to maintaining a desired impedance relationship between the position error and the contact force f_e, we let the target impedance be driven by the contact force error $e = f_r - f_e$, rather than the contact force only. It thus follows that the target force tracking impedance is

$$m\frac{d^2}{dt^2}x_c(t) + b\frac{d}{dt}x_c(t) + kx_c(t) = f_r - f_e \qquad (13)$$

where m, b, k are the positive definite constant matrices of desired mass, damping and stiffness gains respectively, x_c is the commanded position trajectory for the robot position control system.

The fish embryo is identified as a quadratic polynomial [9]

$$f_e = Ax^2 + Bx \qquad (14)$$

where A and B are identified parameters.

Combining (13) with (14) leads to the desired nonlinear interaction dynamics of the micropipette injection system

$$\begin{cases} m\ddot{x} + b\dot{x} + kx = f_d - f_e \\ f_e = Ax^2 + Bx \end{cases} \qquad (15)$$

The standard feedback linearization approach is adopted in constructing a nonlinear controller to track the desired force trajectory. Rewrite (15) in the state space as follows

$$\begin{aligned} \dot{\mathbf{x}} &= \mathbf{f}(\mathbf{x}) + \mathbf{g}(\mathbf{x})\mathbf{u} \\ \mathbf{y} &= \mathbf{h}(\mathbf{x}) \end{aligned} \tag{16}$$

The control input $\mathbf{u}$ is chosen as the reference force f_r, and output $\mathbf{y}$ is chosen as f_e. The control objective is to make the output f_e track the desired input f_r while keeping the states bounded. Differentiating $\mathbf{y}$ yields

$$\dot{\mathbf{y}} = \nabla \mathbf{h}(\mathbf{f} + \mathbf{g}\mathbf{u}) = L_f \mathbf{h}(x) + L_g \mathbf{h}(x)\mathbf{u} \tag{17}$$

where $L_f \mathbf{h}(x)$ and $L_g \mathbf{h}(x)$ denotes the Lie derivative of $\mathbf{h}(x)$ with respect to $\mathbf{f}$ and $\mathbf{g}$, respectively.

Then, the following control law

$$\mathbf{u} = \frac{1}{L_g L_f \mathbf{h}} (-L_f{}^2 \mathbf{h} + v) \tag{18}$$

yields the linear double differential relation between the output and the new input $v = \ddot{\mathbf{y}}$. A diagram of the complete control scheme is shown in Fig. 11.

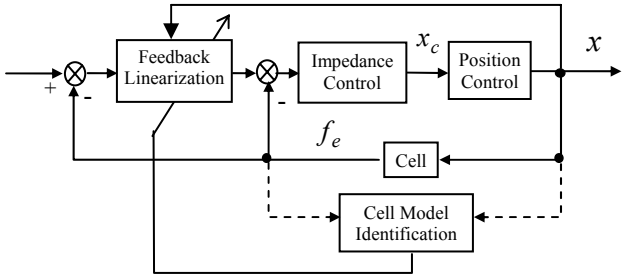

Fig. 11. A block diagram of cell injection control scheme.

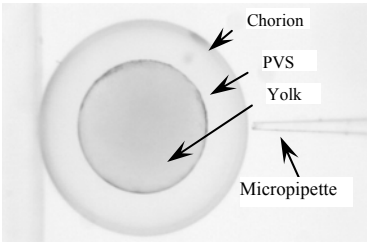

Fig. 12.. The structure of a zebrafish embryo under injection.

IV. EXPERIMENTS

The fish embryo used in our experiments is zebrafish embryo, each with a diameter of 600-800 μm. The structure of zebrafish embryo is shown in Fig. 12. The eggs used in the experiments were collected in accordance with the standard embryo preparation procedures.

In order to evaluate the performance of the force feedback control system, microinjection experiments were performed with different force trajectories. The desired force trajectories were designed in quadratic and ramp types. In the quadratic case, two force trajectories, represented by $f_{d1} = -72t^2$ and $f_{d2} = -120t^2$, were used. In the ramp case, two force trajectories of $f_{d3} = -120t$ and $f_{d4} = -90t$ were used. Considering variations in the mechanical properties of cells at different developmental stages, the embryos were further divided into two stages, i.e. 5 and 7 hours after hatched. A total of 160 embryos were evenly divided into 8 groups as seen in Table 1, for different force trajectories and cell development stages. The outer diameter of the needle tip was about 10 μm.

The tracking performance was evaluated by calculating the relative root mean square error (RRMSE) between the desired force f_d and the measured actual force f_e [23]:

$$RRMSE = \sqrt{\frac{1}{T}\sum_{t=0}^{T} \frac{(f_e(t) - f_d(t))^2}{\max(f_d)^2}} \tag{19}$$

The error is normalized by the maximal value of the desired force to allow an objective comparison among different force trajectories. The average tracking errors and penetration forces of each group are given in Table 2. It is seen that the RRMSE values do not display large difference among the groups. This indicates that the proposed force control algorithm is robust for different types of force tracking and cell development stages.

Table 1: Experiment groups

		Stage1 (5hrs)	Stage2 (7hrs)
Quadratic	f_{d1}	Group 1	Group 2
	f_{d2}	Group 3	Group 4
Ramp	f_{d3}	Group 5	Group 6
	f_{d4}	Group 7	Group 8

Table 2: Average force tracking performance

Group	RRMSE	Penetration force (μN)
1	0.3704	216
2	0.3881	360
3	0.4134	270
4	0.4065	385
5	0.4225	200
6	0.3728	381
7	0.3946	271
8	0.3480	320

As a particular example, Fig. 13 illustrates the desired force, actual force and force tracking error of group 3, where the quadratic force $f_{d2} = -120t^2$ was given as the desired injection force. It is seen that the actual injection force can follow the desired force trajectory rapidly and the force tracking error approaches zero. Furthermore, when the cell was penetrated, the force error changes dramatically, which can be detected easily by setting a threshold and then used as a signal to stop the injection process.

It is worth noting that the injection force to penetrate the cell is different at the different stages. Figs. 14 and 15 illustrate the force control results of group 7 at stage 1 and

group 8 at stage 2, where the desired force $f_{d4} = -90t$ were used in both groups. It can be seen that the penetrated force in stage 2 is bigger than that in stage 1. The same can be found in the force control results of groups 3 and 4, groups 5 and 6, and groups 7 and 8, as seen in Table 2. The reason is that the stiffness of the zebrafish embryo at stage 2 (7 hours) after hatched is bigger than that at stage 1 (5 hours) after hatched according to [15].

V. CONCLUSION

This paper presents a new PVDF force sensor for a force feedback cell injection system. Using the designed force sensor to measure the force applied on the cell, a force control based cell injection system is constructed. The experimental results demonstrate the effectiveness of the micro force sensor and the force based control system for biological cell injection.

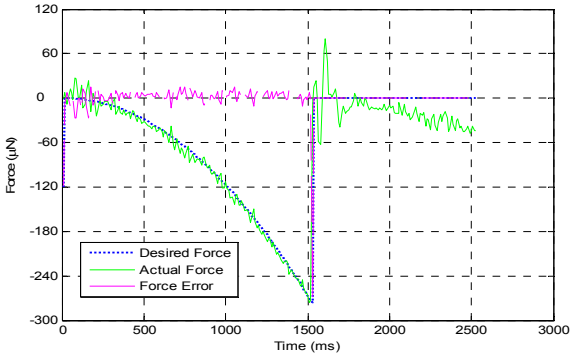

Fig. 13. Force control results of group 3.

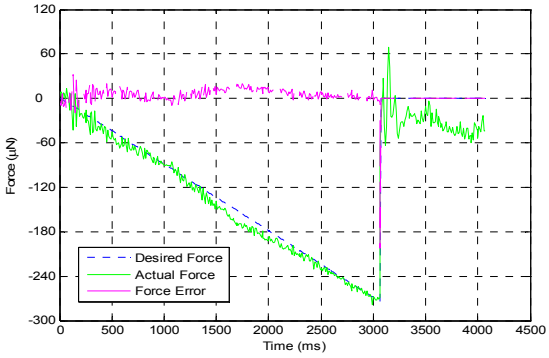

Fig. 14. Force control results of group 7 at stage 1.

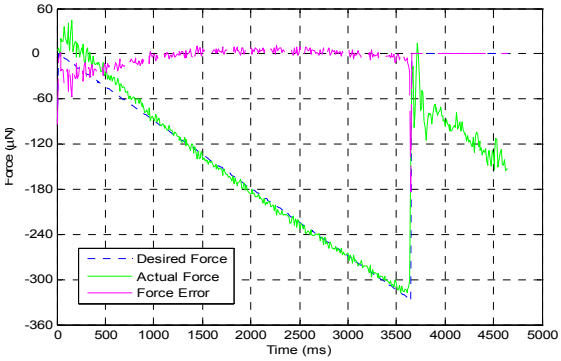

Fig. 15. Force control results of group 8 at stage 2.

REFERENCE

[1] J. C. Lacal, R. Perona, and J. Feramisco, *Microinjection*, Berlin: Birkhauser, 1999.

[2] I. G. Cannell, Y. W. Kong, and M. Bushell, "How do microRNAs regulate gene expression?" *Biochem Soc Trans.*, vol. 36, no. 6, pp. 1224-31, Dec. 2008.

[3] Q. Xu, D. Stemple, and K. Joubin, "Microinjection and cell transplantation in zebrafish embryos," *Methods Mol Biol.*, vol. 461, pp. 513-20, 2008.

[4] Y. Sun, and B. J. Nelson, "Biological cell injection using an autonomous microrobotics system", *International Journal of Robotics Research (IJRR)*, vol. 21, pp. 861-868, 2002.

[5] W. H. Wang, X. Y. Liu, and Y. Sun, "Autonomous Zebrafish Embryo Injection Using A Microrobotic System", *In Proc. of IEEE Conf. on Automation Science and Engineering*, pp.363-368, 2007.

[6] Y. Zhang, K. K. Tan, and S. H. Huang, "Vision-servo system for automated cell injection", *IEEE Tran. on Industrial Electronics*, vol. 56, pp. 231-238, 2009.

[7] Z. Lu, C. Y. Chen, J. Nam, R. Ge and W. Lin, "A micromanipulation system with dynamic force-feedback for automatic batch microinjection", *Journal of Micromechanics and Microengineering*, vol. 17, pp. 314-321, 2007.

[8] H. Huang, D. Sun, J. K. Mills, and S. H. Cheng, "Robotic cell injection system with vision and force control: Towards automatic batch biomanipulation", *IEEE Trans. on Robotics*, vol. 25, no. 3, pp. 727-737, 2009.

[9] Y. Xie, D. Sun, C. Liu, and S. H. Cheng, "A force control based cell injection approach in a bio-robotic system", *IEEE Int. Conf. on Robotics and Automation*, pp. 3443-3448, 2009.

[10] J. Kuncova, and P. Kallio, "Challenges in capillary pressure microinjection", *In Proc. IEEE Int. Conf. of the Engineering in Medicine and Biology Society*, pp. 4998-5001, 2004.

[11] P. F. Indermuhley, G. Schurmann, G. A. Racine and N. F. de Rooij, "Atomic force microscopy using cantilevers with integrated tips and piezoelectric layers for actuation and detection", *J. Micromech. Microeng.*, Vol. 7, pp. 218–220, 1997.

[12] R. Jumpertz, A. V. D. Hart, O. Ohlsson, F. Saurenbach and J. Schelten, "Piezoresistive sensors on AFM cantilevers with atomic resolution", *Journal of Microelectronic Engineering*, Vol. 41-42, pp. 441-444, 1998.

[13] U. C. Wejinya, Y. Shen, N. Xi, and F. Salem, "Force measurement of embryonic system using in situ PVDF piezoelectric sensor", *IEEE Int. Midwest Symposium on Circuits and Systems*, pp.108-112, 2006.

[14] A. Pillarisetti, W. Anjum, J. Desai, G. Friedman, A. Brooks, "Force feedback interface for cell injection", *First Joint Eurohaptics Conference and Symposiumon Haptic Interfaces for Virtual Environment and Teleoperator Systems*, pp. 391–400, 2005.

[15] H. Kim. Y. Sun, and S. Yun, "Mechanical property characterization of the zebrafish embryo chorion", *Proc. IEEE Int. Conf. of the Engineering in Medicine and Biology Society*, pp. 5061-5064, 2004.

[16] Y. Xie, D. Sun, C. Liu and S. H. Cheng, "An adaptive impedance force control approach for robotic cell microinjection", *In Proc. of IEEE Conf. on Intelligent Robots and Systems*, pp. 907-912, 2008.

[17] Y. Tan, D. Sun, W. Huang and S. Cheng, "Mechanical modeling of biological cells in microinjection", *IEEE Trans. on Nanobioscience,* vol. 7(4), pp. 257-266, 2008.

[18] P. P. Benham, R. J. Crawford and C. G. Armstrong, *Mechanics of Engineering Materials*, Longman, 1996.

[19] A.Kuoni, R. Holzherr, M. Boillat, and N. F. Rooij, "Polyimide membrane with ZnO piezoelectric thin film pressure transducers as a differential pressure liquid flow sensor", *J Micromech Microeng* 13(4):S103–S107, 2003

[20] B. Siciliano, and L. Villani, *Robot Force Control,* Springer, 1999.

[21] N. Hogan, "Impedance control: an approach to manipulation: Part I, II, III", *Journal of Dynamical Systems, Measurement, and Control,* vol. 107, pp. 1-16, 1985.

[22] H. Seraji, and R. Colbaugh, "Force tracking in impedance control", *Int. J. of Robotics Research*, vol.16, pp. 97-117, 1997.

[23] R. D. Jones, "Measurement of sensory-motor control performance capacoties: tracking tasks", *The Biomedical Enginerring Handbook*, 2nd ed. Vol. II. Boca Ration: CRC Press, 2000.